Journal of Geophysical Research: Biogeosciences

RESEARCH ARTICLE
10.1029/2018JG004446

Dominant Biological Control Over Upwelling on pCO_2 in Sea East of Sri Lanka

Kunal Chakraborty[1], **Vinu Valsala**[2], **G.V.M. Gupta**[3], **and V.V.S.S. Sarma**[4]

[1]Indian National Centre for Ocean Information Services, Hyderabad, India, [2]Indian Institute of Tropical Meteorology, Pune, India, [3]Centre for Marine Living Resources and Ecology, Ministry of Earth Sciences, Cochin, India, [4]CSIR-National Institute of Oceanography, Regional Center, Visakhapatnam, India

Key Points:
- Phytoplankton bloom, in response to upwelling, decreases pCO_2 in sea east of Sri Lanka (SESL) during summer monsoon
- Relatively shallow nitracline and deep DIC-cline is observed in the SESL
- Removal of pCO_2 due to biological production dominates increase of pCO_2 due to upwelling in SESL

Correspondence to:
K. Chakraborty,
kunal.c@incois.gov.in

Citation:
Chakraborty, K., Valsala, V., Gupta, G. V. M., & Sarma, V. V. S. S. (2018). Dominant biological control over upwelling on pCO_2 in sea east of Sri Lanka. *Journal of Geophysical Research: Biogeosciences*, *123*, 3250–3261. https://doi.org/10.1029/2018JG004446

Received 13 FEB 2018
Accepted 9 SEP 2018
Accepted article online 18 SEP 2018
Published online 11 OCT 2018

Author Contributions
Investigation: Kunal Chakraborty, Vinu Valsala
Resources: Kunal Chakraborty, Vinu Valsala
Supervision: V.V.S.S. Sarma
Writing - review & editing: G.V.M. Gupta, V.V.S.S. Sarma

Abstract Upwelling enhances pCO_2 levels due to injection of carbon-rich water to the surface despite the removal of carbon due to increase in primary production supported by enhanced nutrients. It is hypothesized that in the Bay of Bengal, upwelling may decrease pCO_2 due to existence of low saline and pCO_2-poor waters in the subsurface layer. In order to test this hypothesis, a high-resolution state-of-the-art ocean biogeochemical model (Regional Ocean Modeling System) runs are examined at the sea east of Sri Lanka (SESL) where intense upwelling occurs during summer monsoon (May to August). Upwelling enhances pCO_2 by 34 µatm, whereas decrease in surface temperature and increase in surface salinity reduce pCO_2 by 24 µatm. The estimated net effect of upwelling is an increase in pCO_2 by 10 µatm. In contrast, soft and hard tissues together contribute to a decrease in pCO_2 by 21 µatm suggesting that the biological effect dominates over upwelling, resulting in a net decrease of pCO_2 by 11 µatm in the SESL. This striking contrast between the increase in pCO_2 due to physical dynamics (upwelling) and the removal of pCO_2 due to biological processes is caused by shallow (deep) nitracline (dissolved inorganic carbon-isoline) in the SESL.

1. Introduction

The sea east of Sri Lanka (SESL) is known for its unique physical and biological characteristics during the summer monsoon (SM, June-September; De Vos et al., 2013; Lévy et al., 2007; Vinayachandran et al., 2004). The satellite images during May indicate high surface chlorophyll concentrations in the southern coast of Sri Lanka and Indian Peninsula. High phytoplankton biomass spreads all around Sri Lanka coast during June, which eventually develops as a bloom in July. The SESL also witnesses intense phytoplankton bloom during summer as a response to the nutrient input associated with the Sri Lanka Dome (SLD) and also due to the augmented nutrients from the coast of Sri Lanka and Peninsular India by the intruding SM current (SMC; Vinayachandran et al., 2004).

The nutrients for the phytoplankton bloom in the SESL are supplied by the following mechanisms: (a) a part of nutrients that upwell at the southern coast of Sri Lanka intrudes into the east via the SMC, (b) the open ocean upwelling associated with the SLD nourishes the SESL, and (c) the nutrients upwelling south of Indian Peninsula are advected to the SESL by the intruding SMC (Vinayachandran et al., 2004). The enhancement of nutrients by the intruding SMC is thus an important factor promoting the biological bloom in the SESL. This mechanism supplements the demand of nutrients even in cases where mesoscale eddies are suppressing the upwelling and the SLD (Jyothibabu et al., 2015).

The sediment traps moored close to the southern part of the SESL show that the blooms during June to September are dominated by diatoms with an implication of high biogenic export (~3.6 g $C{\cdot}m^{-2}{\cdot}month^{-1}$; Vidya & Kumar, 2013). Numerical studies on biogenic export indicate that the enhanced primary production reduces the surface ocean pCO_2 of this region by 10 µatm and the corresponding air-sea CO_2 fluxes by 0.1-0.2 g $C{\cdot}m^{-2}{\cdot}month^{-1}$ (Sharada et al., 2008). Observational and numerical simulations have consistently shown the significance of bloom on surface ocean pCO_2 of SESL (Koné et al., 2009; Lévy et al., 2007; Sharada et al., 2008). The pCO_2 is the key oceanic variable that determine the net exchange of CO_2 across the ocean-atmosphere interface. However, a precise quantification of processes responsible for the variability of pCO_2 is still elusive.

Although a large number of studies examined the bloom characteristics of SESL, no significant effort has been made in quantifying the role of bloom in the seasonality of oceanic pCO_2 of SESL

(Valsala & Maksyutov, 2013). The SESL is an important region with respect to the carbon cycle of Bay of Bengal because it is one of the regions where the largest seasonal and interannual variability of surface ocean pCO_2 and air-sea CO_2 fluxes of Indian Ocean are found (Takahashi et al., 2009; Valsala & Maksyutov, 2013). Moreover, as evident from long-term observations, the presence of large phytoplankton biomass and vertical opal and organic carbon flux in the SESL warrants a detailed study of carbon cycle variability in this region, in order to assess the role of bloom in the carbon sink (Jyothibabu et al., 2015; Vidya & Kumar, 2013). Hence, in this study we have examined the controlling factors of surface ocean pCO_2 and air-sea CO_2 flux variability of SESL during SM.

The significance of assessing the role of bloom in pCO_2/CO_2 fluxes of SESL can be conceived as follows. The compilation of various model results and synthesized estimates clearly show that the northern Indian Ocean is a net source of CO_2 to the atmosphere with an exception of Bay of Bengal, which is a mild sink in which ocean biology plays an integral role (Lévy et al., 2007; Sarma et al., 2012, 2013; Sharada et al., 2008; Valsala & Maksyutov, 2013). This is further confirmed by high volume export of organic carbon to deep waters in the SESL region (Vidya & Kumar, 2013). This is unique compared to the rest of the Bay of Bengal, which is relatively less productive in the summer season mostly due to the lack of supply of nutrients across the stratified upper ocean and shallow photic depth due to high suspended load (Madhupratap et al., 2003; Prasanna Kumar et al., 2002). In contrast the eddy-mediated biological pump is evident during most of the year (Sabu et al., 2015; Sarma et al., 2016). SESL, on the other hand, experiences phytoplankton blooms owing to the SLD formation and SMC intrusion. Therefore, assessing the oceanic pCO_2 variability of this highly biogenic export region is of prime importance to the carbon cycle of the Bay of Bengal.

There has been no routine monitoring of surface ocean pCO_2 of the Bay of Bengal except for a few research-based cruises focusing on the coastal areas of the Bay (Sarma et al., 2012, 2015). A data-based assessment of carbon cycle of the upper ocean Bay of Bengal is thus not feasible and that forces studies to resort on biogeochemical models (Sarma et al., 2013). Therefore, by using a high-resolution physical-biogeochemical coupled model, we have investigated pCO_2 variability and its controlling mechanisms in the SESL region.

2. Data and Methods

We have used Sea-viewing Wide Field-of-view Sensor satellite's 8-day-averaged chlorophyll-a (Chl-a) data product with approximately 9-km spatial resolution from National Oceanic and Atmospheric Administration Coast Watch data portal. Further details for Sea-viewing Wide Field-of-view Sensor and Aqua missions can be accessed through the Ocean Color portal managed by the National Aeronautics and Space Administration's Goddard Space Flight Center. These data are normalized to match spatial resolution of the model for comparison.

A Bio-Argo profiling float (WMO No. 2902086) equipped with temperature and salinity (SBE41CP), dissolved oxygen (Aanderra Optode 4330), and chlorophyll fluorescence (WET Labs FLBB), deployed in the central Bay of Bengal, at the end of December 2012, near 12.2°N, 88.7°E is used for assessment of the model simulated Chl-a variability in the subsurface waters of the Bay of Bengal. The daily vertical profiles of Chl-a were recorded by the float from 30 December 2012 to 17 January 2013. Subsequently, the mission cycle was changed to 5 days. These floats were manufactured by Sea-Bird Electronics and used in the Indian ARGO project managed by the Indian National Centre for Ocean Information Services (INCOIS). The floats acquire data during their ascent at predetermined depths. In the present study, Bio-Argo profiles in the upper 100 m of the water column between 1 January 2013 and 31 December 2015 are used. The data quality of the profiles is checked following Takeshita et al. (2013). Takahashi et al. (2009) prepared monthly climatological maps of pCO_2 (Takahashi climatology) using the available global oceanic pCO_2 observations. These maps are used to assess the capability of the model simulated surface ocean pCO_2.

2.1. Model Description

A fully coupled high-resolution physical-biogeochemical model has been successfully configured for the entire Indian Ocean basin (30°S to 30°N; 30°E to 120°E) using Regional Ocean Modeling System (ROMS) version 3.7 (Haidvogel et al., 2008).

The model has a horizontal grid resolution of 1/12° (approximately 9 km) and uses 40 vertical layers in a terrain-following *s* coordinate system. In the physical part of the model setup, the narrow channel between India and Sri Lanka is kept as closed and isolated land mask points were removed. The shallow Mallacca strait

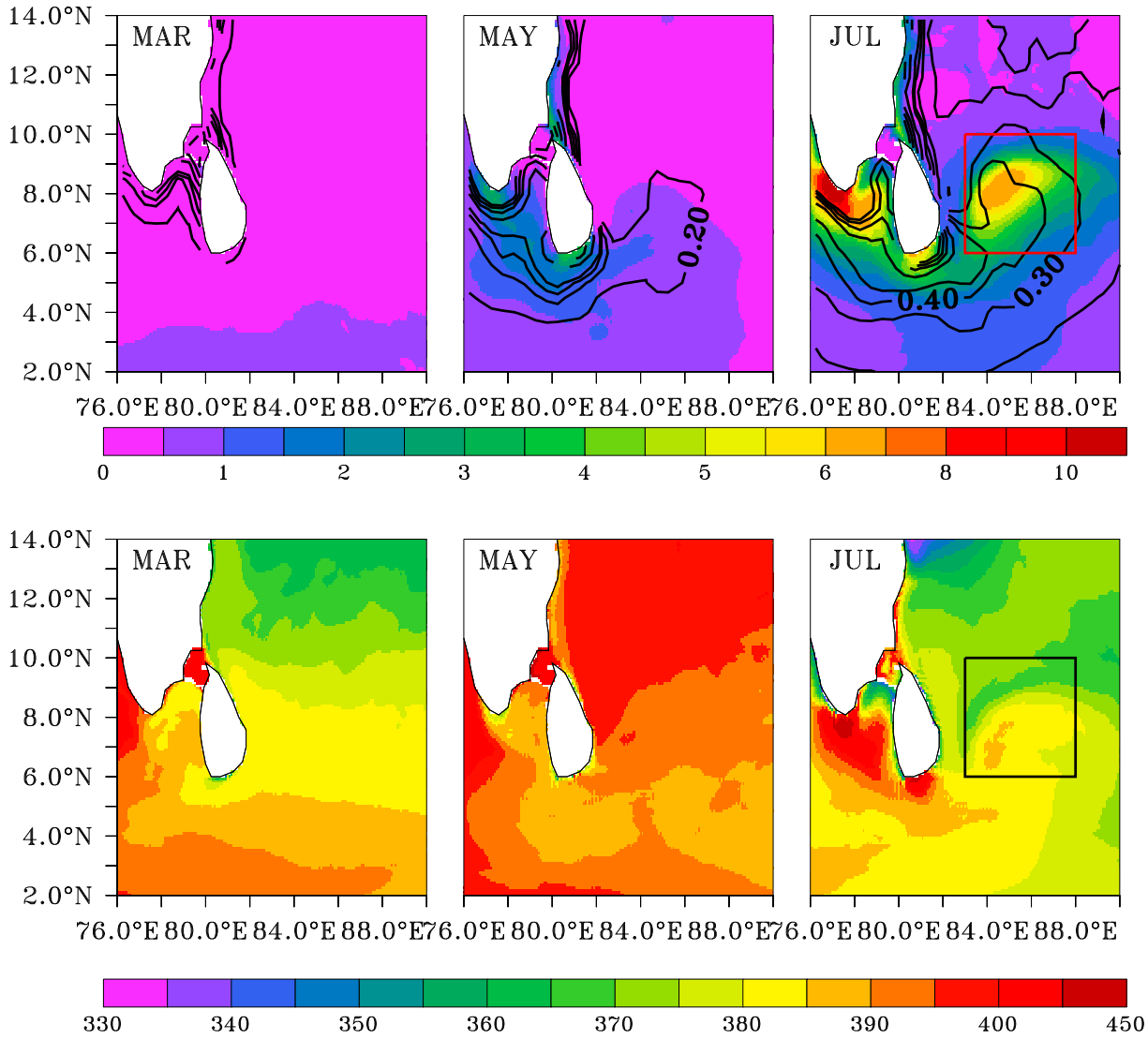

Figure 1. (top row) The model-derived Chl-a (shade; mg/m^3) and corresponding satellite observations (contour; mg/m^3), (bottom row) Model simulated monthly mean pCO_2 (μatm) for March, May, and July in the sea east of Sri Lanka. The box (83–88°E, 6–10°N) represents the intruding shape of Chl-a in the sea east of Sri Lanka.

and the part of the South China Sea are also removed from the model grid. On the western and northern continental land boundaries, no slip and no normal flow boundary conditions are applied. The lateral boundaries in the east and south are kept open. It is challenging to configure global models with sufficiently fine horizontal and vertical resolutions due to computational limitations. A global model with coarse resolution cannot capture all fine-scale variability in the regional oceans. Also, the inherent inaccuracies in initial and boundary conditions can cause issues such as numerical drifting in model simulations. Therefore, the one-way nested modeling approach is adopted in which a global ocean general circulation model provides boundary data to a regional model that is further coupled to an ecosystem model (Shulman et al., 2003). This approach utilizes strong relaxation at the open boundaries, but weaker relaxation in shallow waters and productive zones to allow the model to respond more freely to surface atmospheric forcing. The K-Profile Parameterization scheme of Large et al. (1994) is used to represent vertical mixing. Biharmonic viscosity and diffusion schemes are chosen for horizontal mixing (Griffies & Hallberg, 2000).

The tracer fields (temperature and salinity), sea surface height, and the components of momentum are initialized on 1 January 2003 with the state of the ocean as available in the Global Ocean Data Assimilation System, configured at the INCOIS (Ravichandran et al., 2013). The weekly averaged boundary on interannual

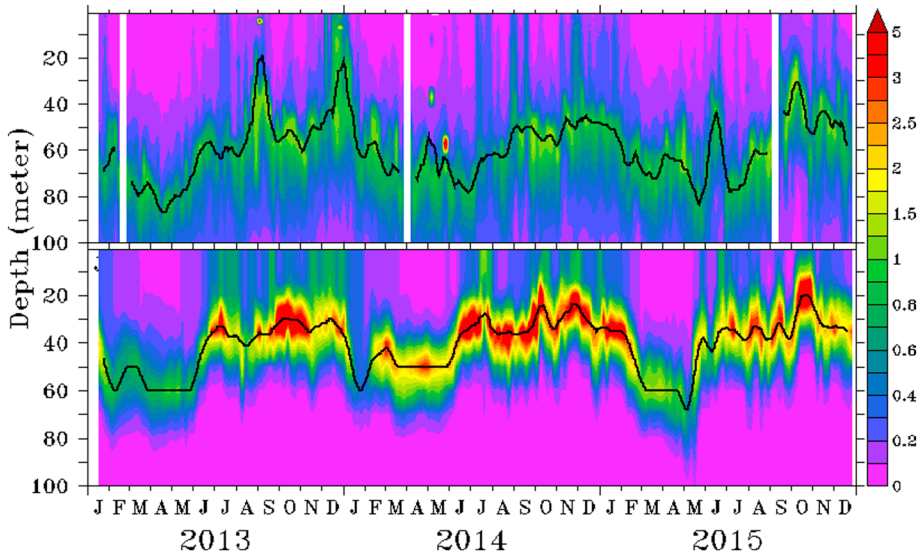

Figure 2. Comparison between model (bottom panel) simulated chlorophyll-a (mg/m^3) concentrations against observations (top panel) made by Bio-Argo float (WMO No. 2902086) deployed in the south central Bay of Bengal (12.2°N, 88.7°E).

time scale derived from the Global Ocean Data Assimilation System was prescribed for the tracers, sea surface height, and momentum fields along the east and south lateral boundary. The National Centre for Medium Range Weather Forecast (New Delhi, India) has developed a data assimilated Global Forecast Systems (GFS) at a horizontal resolution of 0.25° which provides real time forecasts of forcing fields to force ocean models configured at the INCOIS (Rajagopal et al., 2012). Six-hourly analyzed atmospheric forcing fields obtained from the National Centre for Medium Range Weather Forecast are used to force the model setups during 1 January 2003 to 31 December 2017. Atmospheric forcing component includes air pressure and temperature at 2 m, net shortwave and longwave flux, rain fall rate, and wind velocity. Surface heat and momentum fluxes are internally calculated by ROMS using the bulk parameterizations of Liu et al. (1979), Fairall, Bradley, Godfrey, et al. (1996), and Fairall, Bradley, Rogers, et al. (1996).

The biological component of our coupled setup consists of the nitrogen cycle model with parameterized sediment denitrification described by Fennel et al. (2006). The nitrogen cycle model includes seven state variables viz., phytoplankton, zooplankton, nitrate, ammonium, large and small detritus classes with nitrogen concentration, and phytoplankton chlorophyll. The time rate of change of concentration of each state variable describes the balance of advection-diffusion and source-sink terms among the related state variables of the nitrogen cycle (Fennel et al., 2006). The biological model also resolves the full carbon cycle. The model carbonate chemistry is described in the coupled setup following (Zeebe & Wolf-Gladrow, 2001) and (Fennel et al., 2008). The full carbon cycle is represented in the model using four state variables viz., alkalinity, dissolved inorganic carbon (DIC), and large and small detritus class with carbon concentration. The dynamics of DIC includes the primary production and respiration as sinking and source processes respectively following redfield stoichiometry besides gas exchange at the air-sea interface. The biogeochemical processes, such as calcite formation and dissolution, nitrate uptake and regeneration, and sulfate reduction are represented in the dynamics of alkalinity. The air-sea gas exchange of CO_2 does not have any impact on the dynamics of alkalinity (Millero et al., 1998). The partial pressure of carbon dioxide (pCO_2) is calculated in the surface layer as described in Fennel et al. (2008). Oxygen is included as model tracer and biogeochemical dynamics of oxygen is described in the model following Fennel et al. (2013).

The biological variables are initialized using the climatological state of January generated during climatological run of the coupled setup. Considering the unavailability of sufficient observations along the boundaries, the monthly climatological boundary derived from the NODC World Ocean Atlas 2013 is prescribed for the nitrate, oxygen, DIC, and alkalinity, whereas small uniform values along the east and south lateral boundary are prescribed for the remaining state variables. Daily averaged output has been stored from 1 January 2003 to 31 December 2017 for the analysis.

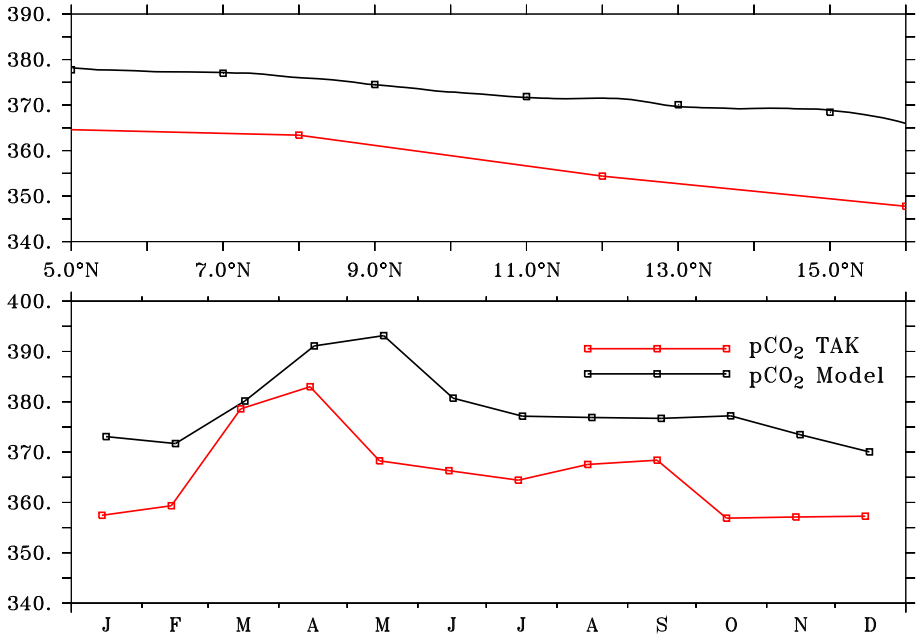

Figure 3. (top panel) Comparison of model-simulated surface ocean pCO_2 (µatm) with Takahashi et al. (2009) climatology at 90°E. (bottom panel) Comparison of the same but averaged over the box (83-88°E and 6–10°N) in the sea east of Sri Lanka.

3. Results and Discussion

The evolution of surface Chl-a concentration surrounding the Sri Lanka and SESL are faithfully reproduced in the model (Figure 1, top). The model simulated monthly variability of pCO_2 (µatm) for March, May, and July in the SESL is depicted in Figure 1 (bottom). During March, no significant upwelling is observed in the sea surrounding Sri Lanka resulting in low Chl-a concentrations. By early May, winds change the direction and the southern coast of Sri Lanka experiences upwelling (Vos et al., 2014) and subsequent enhancement in the Chl-a concentrations is observed from the satellite imageries. The model faithfully captures this signal. Figure 1 (top) compares the mean satellite Chl-a concentration for the months of March, May, and July with that of the model. The comparison shows reasonably good agreement except a slight difference in amplitude. The contours of Chl-a surrounding Sri Lanka and its intruding shape to the SESL is captured in the model fairly well. The upwelling sets in the southern peninsula of India by May–June and propagates northward along the eastern Arabian Sea shelf during SM. The evolution of model simulated upwelling and phytoplankton bloom over its southern shelf are in good agreement with the observations reported by Gupta et al. (2016).

A similar comparison of model Chl-a concentrations with that derived from a Bio-Argo float (WMO No. 2902086) deployed in the south central Bay of Bengal further evaluates the capacity of the model to reproduce the observed biological variability in the region (Figure 2). Although the float did not traverse strictly through the SESL region, a comparison to the nearest available Bio-Argo float increases the confidence in our model performance. A subsurface Chl-a maxima at about 40–60 m and its spatial variability from January 2013 to December 2015 is well captured in the model (Figure 2). To facilitate the analysis, the model outputs are extracted at the time and location (nearest grid point) of Argo profiles. The undulations in the simulated Chl-a spatial variability is well comparable with the observations albeit the magnitude is over estimated in the model.

A similar attempt to compare the model surface ocean pCO_2 of Bay of Bengal with the observations (Takahashi et al., 2009) suggest that except for a systematic bias of 10 µatm throughout the basin from 5°N to 16°N, the overall gradient of pCO_2 from head Bay to 5°N is reproduced well in the model (Figure 3). Nevertheless, as the pCO_2 observations compiled in Takahashi et al. (2009) is centered for a year in the middle of 2000s; therefore, the basin-wide bias of 10 µatm can be readily attributed to the increasing DIC concentration that has been added in the recent times to the ocean via increased anthropogenic forcing (Sarma et al., 2015).

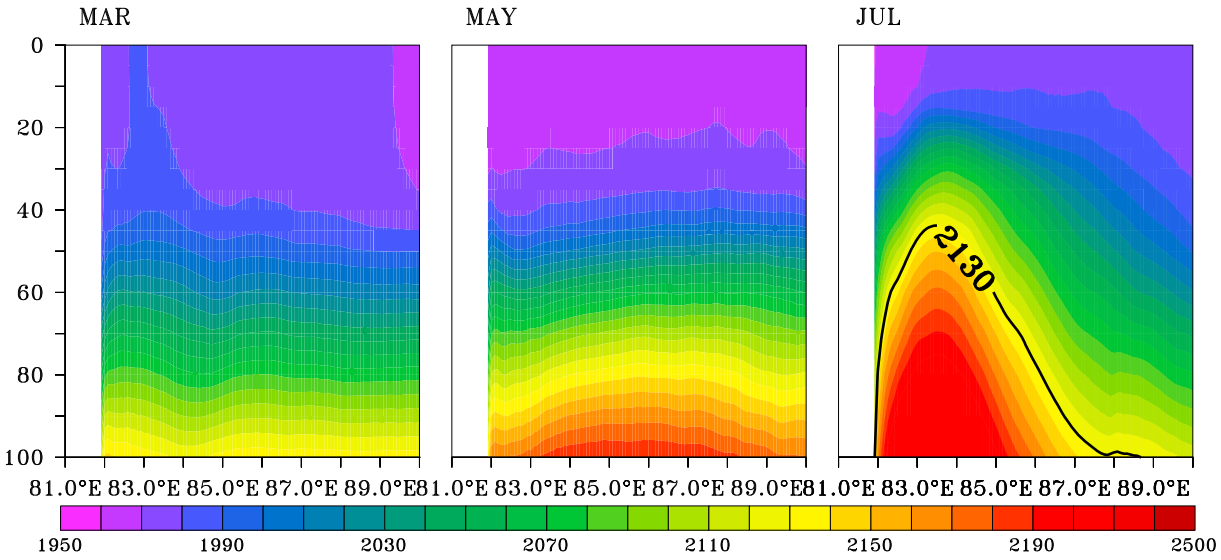

Figure 4. Model simulated monthly mean of the vertical section of dissolved inorganic carbon (mM/m^3) at 7°N for March, May, and July in the sea east of Sri Lanka.

Higher pCO_2 values are noticed during April-May as compared to other months by 10–30 µatm (Figure 3, bottom). The onset of the phytoplankton bloom draws down the pCO_2 from June to September by 10–15 µatm. The model fairly captures observed seasonality of pCO_2 in the SESL region.

Considering the dynamics and associated biological response during SM (June to September), upwelling of subsurface waters in the SESL favors (a) decrease in pCO_2 by the enhanced biological production due to intrusion of "nutrient-rich" subsurface water via SMC, (b) vertical mixing that enhances surface DIC/pCO_2 levels due to pumping of enriched waters from below (Figure 4), (c) change in sea surface temperature (SST) associated with the SLD (Vinayachandran et al., 2004) and SMC intrusion (De Vos et al., 2013) that alters solubility pump of the region (Figure 5), and (d) variation in air-sea exchange (Udayshankar, 2015) may intricately alter the pCO_2 levels. The effect of all these processes eventually determine the net pCO_2 variability of the region.

The net pCO_2 variability of surface ocean is also controlled by abiotic factors or buffer chemistry of surface carbon and usually follows the pattern of SST especially in the region like Bay of Bengal where biological production is relatively weak (Prasanna Kumar et al., 2004). The change in pCO_2 of the SESL region gradually follows the evolution of SST in the region (Figure 4) from January to June when the biological pump is weak as evidenced from satellite Chl-a concentrations (Figure 1, top). However, from July to September the variability of pCO_2 of the SESL is not in phase with that of the SST indicating decoupling of SST-pCO_2 relation by the interplay of biology and physical dynamics (upwelling) of this region. The spatial pattern of evolution of pCO_2 from March to July shows that the surface ocean pCO_2 in the SESL region has coherent "trends" with that of the observed satellite Chl-a concentrations by July (Figure 1). The relatively higher sinking biogenic fluxes from this region (Vidya & Kumar, 2013) further infers the significant role of biological pump in regulating surface ocean pCO_2. This affirms our hypothesis that the intricate relation between surface ocean dynamics and biology has to be analyzed in tandem for identifying the mechanisms responsible for the variability of pCO_2 during the bloom.

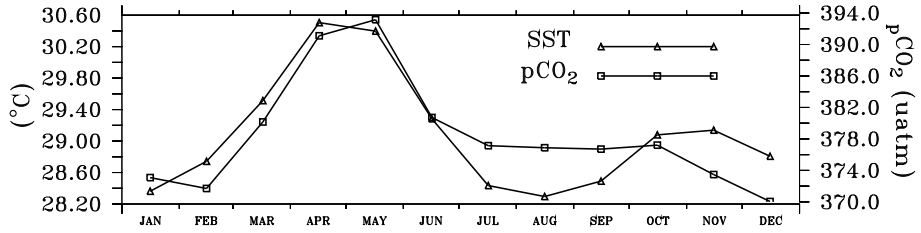

Figure 5. Seasonal cycle of model-derived pCO_2 (right axis) and sea surface temperature (SST, left axis) averaged over the box (83–88°E and 6–10°N) in the sea east of Sri Lanka.

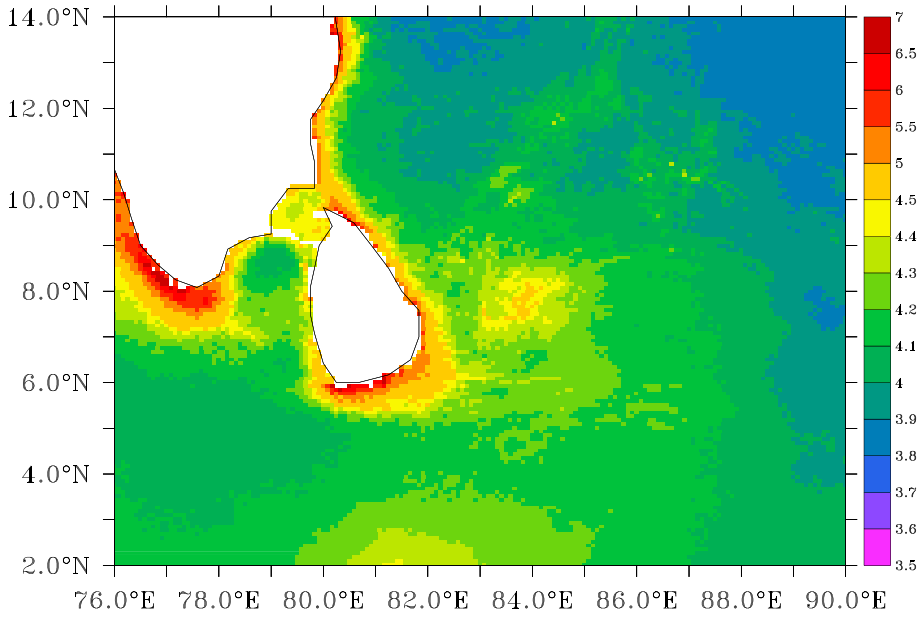

Figure 6. Root-mean-square error (RMSE) of the net pCO_2 after reconstructing it by offline abiotic pump model. RMSE is calculated from the difference of reconstructed pCO_2 and pCO_2 of the original model simulation for the sea east of Sri Lanka region. RMSE is calculated from daily data of entire period of model simulation.

The component equation depicting the total variability of surface ocean pCO_2 as represented elsewhere (Takahashi et al., 2009; Valsala & Maksyutov, 2013) is as follows:

$$\frac{dpCO_2}{dt} = \frac{\partial pCO_2}{\partial DIC}\frac{dDIC}{dt} + \frac{\partial pCO_2}{\partial ALK}\frac{dALK}{dt} + \frac{\partial pCO_2}{\partial SST}\frac{dSST}{dt} + \frac{\partial pCO_2}{\partial SSS}\frac{dSSS}{dt} \quad (1)$$

The left term of the equation represents the total evolution of pCO_2. The terms on the right side represent the pCO_2 variability due to dynamics of surface ocean DIC (biotically linked to alkalinity), alkalinity (ALK), temperature (SST), and salinity (SSS), respectively.

In order to segregate the individual components in the total pCO_2 seasonal cycle, we did an offline component analysis. The coupled physical-biogeochemical model simulated daily averaged outputs of DIC, ALK, SST, and SSS for the entire simulation period were considered for the analysis. The solubility abiotic routines of the carbon chemistry model was run offline for the entire simulation period with daily averaged surface DIC, ALK, SST, and SSS and the corresponding pCO_2 is reconstructed. The reconstruction of net pCO_2 results in insignificant residual error (± 2 μatm) as is evident in the root-mean-square error analysis (Figure 6). In the subsequent offline abiotic runs, we supplied the annual mean of a given parameter at each grid and reproduced the net pCO_2. The supply of annual mean for a particular variable to run the abiotic model in offline means that we were eliminating the impact of a particular term in the seasonality of pCO_2 in the above equation at each run. Therefore, the difference between reconstructed control pCO_2 and the pCO_2 of sensitivity runs gave the contribution of individual components in the net pCO_2 variability. Furthermore, we calculated the tendency of control pCO_2 per month and estimated its daily standard deviation as standard error. This procedure is also applied for individual reconstruction of pCO_2 for each variable. Four such sensitivity abiotic carbonate pump runs have been done with the supply of respective annual mean of DIC, ALK, SST, and SSS each time.

The change in the total ocean biology has a significant contribution to the pCO_2 variability as well. The total biological contribution is considered to be the summation of individual contribution of soft and hard tissues. In order to obtain the individual contribution of the soft and hard tissues, the methodology prescribed by Louanchi et al. (1996) is used. The details of the separation of soft and hard tissue pumps from the model solutions are given in Appendix A

The offline component analysis quantified the contribution of individual term in equation (1) in the net pCO_2 variability of SESL region, while the quantification of individual contribution of soft tissue and hard tissue is

Table 1
Monthly pCO_2 Tendency Due to Variability in Individual Components According to Equation (1)

Month	CTRL	DIC	SST	ALK	SSS
MAY	−5.55 ± 0.88	−9.68 ± 3.42	4.73 ± 0.49	−2.99 ± 1.86	−8.43 ± 0.91
JUNE	−8.33 ± 0.43	−20.84 ± 3.16	7.69 ± 0.51	−1.62 ± 2.07	−10.47 ± 0.44
JULY	−1.94 ± 0.38	−15.91 ± 1.94	6.24 ± 0.83	7.73 ± 1.62	−4.48 ± 0.38
AUGUST	0.03 ± 0.67	−3.68 ± 1.77	−0.79 ± 1.24	5.66 ± 1.68	−1.95 ± 0.66
Sum of CTRL — Sensitivity	0	34.32 ± 10.29	−33.66 ± 3.07	−24.58 ± 7.23	9.54 ± 2.39

Note. CTRL indicates the net pCO_2 tendency in the control reconstruction of pCO_2 by the abiotic pump runs. Surface ocean dissolved inorganic carbon (DIC; mM/m^3), alkalinity (ALK, mEq/m^3), temperature (sea surface temperature, SST; °C), and salinity (sea surface salinity, SSS; PSU) represent the contribution by individual components in the pCO_2 variability. The error shows the uncertainty in the mean of respective months. *(CTRL — individual components) gives the net impact of each variable*. Units are in microatmospheres.

done following equations (A2) and (A3) in Appendix A. A summary of monthly averaged contribution of individual components to pCO_2 variability and their uncertainties are given in Table 1. The monthly contribution of soft and hard tissues are listed in Table 2. The climatology of the sensitivity runs are then contrasted with the climatology of control pCO_2 (Figure 7).

The upwelling effect influences pCO_2 in two opposite directions — (1) input of CO_2-rich subsurface waters to surface and (2) increase in solubility of CO_2 due to injection of cool and saline waters resulting in decrease in pCO_2. These two effects counteract each other; hence, the net effect can be taken as physical effect. For instance, decrease in SST between May and August reduces pCO_2 of the SESL by 33.6 µatm, whereas increase in salinity enhances pCO_2 levels by 9.5 µatm (Table 1). This is due to cooling of the sea surface and enhanced salt content by SMC intrusion of upwelled water from south of Sri Lanka as well as by the upwelling related to the SLD (De Vos et al., 2013; see Table 1 for mean and root-mean-square error). Therefore, the net solubility effect is a reduction of pCO_2 by 24.1 µatm. In contrast, vertical mixing caused by upwelling enhanced monthly pCO_2 by 4.1, 12.5, 13.9 and 3.7 µatm, respectively, from May to August, with a total of 34.2 µatm, due to intrusion of SMC and upwellling due to SLD. Therefore, the net effect was an increase of 10 µatm due to direct input of CO_2 through vertical mixing caused by upwelling and change in pCO_2 due to solubility variations (Table 1).

Figure 4 suggests that the effect of hard tissue is smaller than that of soft tissue during study period. The effect of soft tissue formation is small during April (0.1 µatm) and then increases to −10.1 µatm in July and eventually decreases to −7.1 µatm in August. In contrast, the hard tissue formation increases pCO_2 by <1.3 µatm during our study period. The net biological effect (both hard and soft tissues) decreases monthly pCO_2 by 1.2, 5.1, 8.8, and 5.9 µatm respectively during May–August, with a total net decrease of pCO_2 by 21 µatm (Table 2). Therefore, the net effect of upwelling is to decrease pCO_2 by 11 µatm (21 µatm decrease by biology and 10 µatm net increase by vertical processes). In spite of the net contribution of physical dynamics being close to zero, the biological impact remains high (6 µatm) during August due to the prolonged biological response (see; Lévy et al., 2012, for phase lead-lag between biological and solubility pumps at submonthly scales). Earlier studies pointed out that the impact of mixing on pCO_2 during a cyclone is almost negligible as mixing initially increases pCO_2, whereas biological removal compensates the physical mixing over a period of month (Lévy et al., 2012). When nutrients are pumped, the change in pCO_2 is controlled by both mixing (which increases pCO_2) and solubility (cooling of the sea surface decrease pCO_2 and increases in salt content increases pCO_2). The balance of these controls lead to the net pCO_2 change. In presence of sufficient nutrients, phytoplankton

Table 2
Monthly Individual Contribution of Soft and Hard Tissues on pCO_2 Following the Equations (2) and (3) of Louanchi et al. (1996)

Month	Soft tissue	Hard tissue
May	−0.84 ± 0.10	−0.34 ± 0.01
June	−5.44 ± 0.30	0.30 ± 0.05
July	−10.16 ± 0.51	1.37 ± 0.08
August	−7.06 ± 0.46	1.16 ± 0.07
Total	−23.5 ± 1.37	2.49 ± 0.21

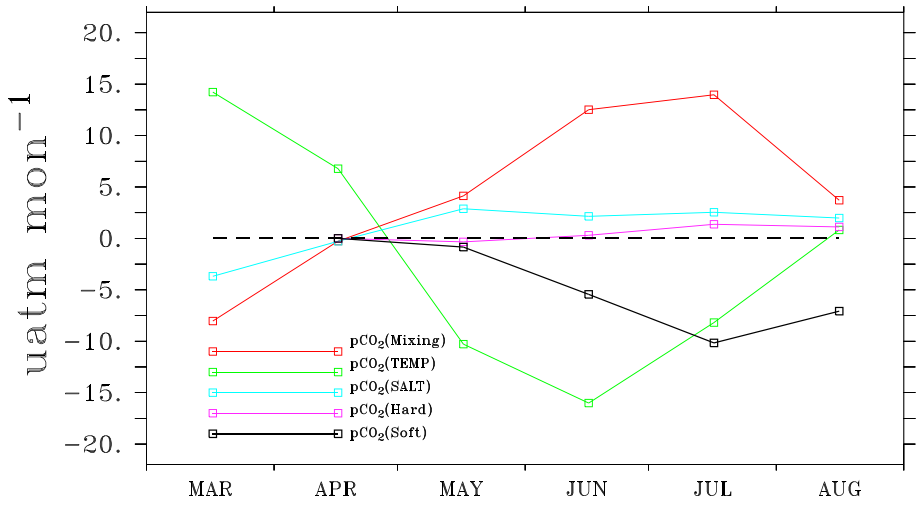

Figure 7. The contribution of the individual components (dissolved inorganic carbon [vertical mixing], sea surface temperature, sea surface salinity, and total biology [soft tissue and hard tissue]) on net pCO_2 variability during March to August in the sea east of Sri Lanka region. Black dotted line represents the control run, red line represents the contribution of dissolved inorganic carbon (vertical mixing), green line represents the contribution of sea surface temperature, cyan line represents the contribution of sea surface salinity, black line represents the contribution of biological soft tissue, and magenta line represents the contribution of biological hard tissue.

production dominates and decreases the pCO_2. Later, once the production weakens, respiration dominates and increases the pCO_2. The DIC, on the other hand, counteracts the impact of net pCO_2 change as suggested by Lévy et al. (2012). Nevertheless, the averaged monthly responses that we reported here average out the possible shorter time scale lead-lag responses of biology and solubility pumps on the net pCO_2.

A conspicuous pCO_2 variability by DIC and SST is noticeable during July. At the peak of the bloom, the augmentation effect of DIC on pCO_2 appears to be strongest among all months examined here. The impact of SST starts weakening during July, while the impact of mixing strengthens. The concomitant biological impact during July indicates its role in draw down of pCO_2. The significant decrease in pCO_2 is further confirmed by significant increase in sinking carbon flux in SESL (see; Jyothibabu et al., 2015; Vidya & Kumar, 2013, for the sediment trap data) that may further enhance the DIC while decreasing the ALK. Therefore, the increase in pCO_2 due to DIC (during July) and decrease in pCO_2 due to alkalinity support the role of both soft tissue and carbonate pumps, leading to dominant biological exports in the SESL region. It is worth mentioning that the sediment traps were mounted 800 m below the surface to explore the variability of biogenic carbonate fluxes, whereas the dome shape of DIC is observed around 100 m. Therefore, we infer that the variations in upper ocean DIC are caused mostly by upwelling waters rather than carbonate pump which is located below the depth of upwelled waters. High-resolution sediment trap measurements are required to further separate the role of soft tissue and carbonate pumps on pCO_2 in the SESL.

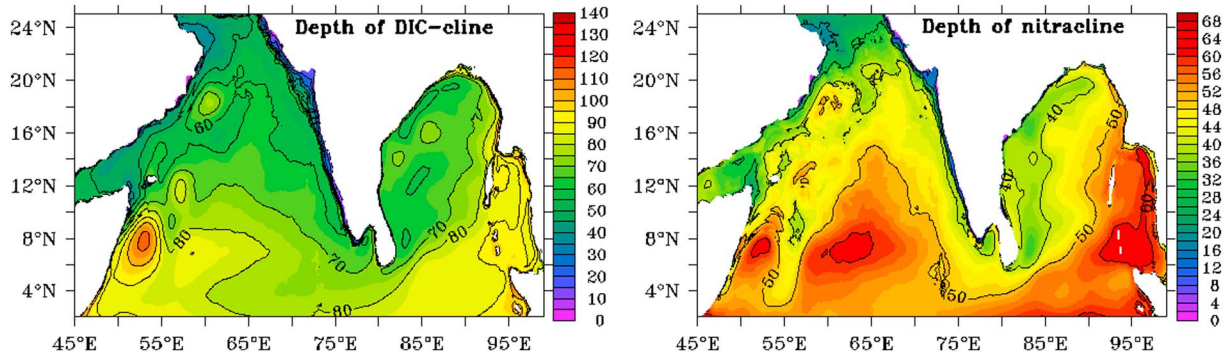

Figure 8. Annual mean depth of 2,100-mM dissolved inorganic carbon (DIC)-isoline (DIC-cline) and 2-mM nitrate isoline (nitracline) in the northern Indian Ocean.

The dominance of biological effect over physical dynamics in the SESL, which is a part of the Bay of Bengal, is in contrast with the domination of physical effect observed in the Arabian Sea, equatorial Indian Ocean, and south tropical Indian Ocean (Goyet et al., 1998; Louanchi et al., 1996; Sarma et al., 2000). Despite the supply of both DIC and nutrients, it is interesting to know why biological processes dominate over physical dynamics in the Bay of Bengal. In order to examine this, the depths of 2,100-mM DIC-isoline (DIC-cline) and 2-mM nitrate isoline (nitracline) is plotted both in the Arabian Sea and Bay of Bengal (Figure 8). It is noticed that depth of DIC-cline is deeper while nitracline is shallower in the Bay of Bengal than Arabian Sea due to shallow mixed layer and existence of relatively fresh water in the upper layers due to river discharge. This results in lower DIC and release of nutrients at shallower depth (below mixed layer) through decomposition of organic matter. This may result in pumping of low DIC and higher nitrate to the mixed layer in response to upwelling in the Bay of Bengal compared to Arabian Sea, which leads to the dominance of biological production over mixing in the former basin. Our study suggests that in CO_2 dynamics, biological processes dominate over physical processes in the SESL and lead to a net decrease of 11 μatm in pCO_2 during the SM.

4. Summary and Conclusions

Based on state-of-the-art high-resolution ocean biogeochemical model (ROMS), the variability in carbon cycle in one of the prominent phytoplankton bloom areas of the Bay of Bengal in the Indian Ocean is studied. Focusing on the variability of pCO_2, as a key variable depicting the air-sea equilibrium of CO_2 in this region, for the first time, we have demonstrated how biology dominates over physical dynamics in the SESL region. Over global ocean, typically upwelling and mixing effects predominantly control pCO_2 over other effects, including biology, as mixing brings CO_2-rich waters to surface. In contrast, it is noticed that higher nutrients are brought to the surface compared to DIC due to low saline waters in the upper 100 m resulting from river discharge. This leads to deep DIC-cline, as fresh water contains lower DIC than seawater, and shallow nitracline compared to the Arabian Sea and other regions in the Indian Ocean.

Several cyclonic eddies and seasonal cyclones/depressions (summer and postmonsoon) form in the Bay of Bengal, and they are expected to churn the upper ocean resulting in pumping of DIC- and nutrient-rich waters to surface. It has been hypothesized in earlier studies that the net effect of tropical cyclones, due to mixing and biological response, on surface pCO_2 may be balanced over time, if phase lag is considered. Our study, in contrast, suggests that such balance may be unlikely due to less DIC input compared to nutrients resulting in dominant biological removal of atmospheric CO_2. However, more work is required to confirm our hypothesis on modulation of carbon cycling due to physical dynamics in the Bay of Bengal vis-a-vis Arabian Sea.

Appendix A: Segregation of Individual Contribution of the Soft and Hard Tissue Pumps

The change in pCO_2 due to biology is derived from DIC and ALK variations linked to the biomass production and the calcite formation in the euphotic layer and taken from Louanchi et al. (1996). These variations are expressed using the following equations:

$$\left(\frac{\partial DIC}{\partial t}\right)_{\text{biology}} = \left(\frac{\partial N}{\partial t}\right)_{\text{biology}} * RCN - S_{\text{biology}} \tag{A1}$$

$$\left(\frac{\partial ALK}{\partial t}\right)_{\text{biology}} = -2 * S_{\text{biology}} \tag{A2}$$

The first term of the right-hand side of equation (A2) represents the variation in nutrients with time resulting from photosynthesis, mortality, and respiration, converted in terms of carbon unit from the C:N redfield ratio *RCN* (Redfield et al., 1963). The rate of change in nutrients is computed at each time step according to the following equation:

$$\left(\frac{\partial N}{\partial t}\right)_{\text{biology}} = -(u - r * q) * Chl * RN \tag{A3}$$

where u is the growth rate which depends on the maximal growth rate u_m and on the single nutrient following a Michaelis-Menten formulation [$u = u_m * N/(N + K_m)$], where K_m is the half-saturation constant, r is the

removed factor, and q is the respiration, mortality, and grazing rate. The u and q are calculated at each time step using the following equation:

$$\left(\frac{\partial Chl}{\partial t}\right)_{\text{biology}} = (u - q) * Chl \tag{A4}$$

where $\partial Chl/\partial t$ is the rate of change in chlorophyll. RN is the N:Chl redfield ratio. The second term of the right-hand side of equation (A2) represents the temporal variation of the global calcite concentration which is expressed as 20% of the total exported production (P_{export}).

$$S_{\text{biology}} = 0.2 * (\partial P_{\text{export}}/\partial t) \tag{A5}$$

Again, the exported production P_{export} consists of two parts of inorganic and organic carbon and is computed in terms of carbon at each time step by

$$(\partial P_{\text{export}}/\partial t) = (1 - r) * q * Chl * RCC \tag{A6}$$

where RCC is the C:Chl redfield ratio.

References

Acknowledgments
We are grateful to the anonymous reviewers for their careful reading, constructive comments, and helpful suggestions, which have helped us to significantly improve the presentation of this work. K. C. earnestly thanks MDG members for the help in setting up the ROMS simulations. K. C. acknowledges the DMG and CWG of the INCOIS, respectively, for providing Bio-Argo data and necessary support to run ROMS in INCOIS-HPC. K. C. gratefully acknowledges the Director, INCOIS, for his encouragement and unconditional help. We are thankful to Arya Paul and Almeida Celsa Margaret of INCOIS, Hyderabad, and Shikha Singh of IITM, Pune, for helping us in improving the English of the manuscript. This work has been carried out under the Ocean-Modeling, Data Assimilation and Process SpeCific ObservaTions (O-MASCOT) program coordinated by the Indian National Centre for Ocean Information Services (INCOIS) and funded by Ministry of Earth Sciences (MoES; Ref: MoES/36/OOIS/O-MASCOT/2017). We thank NOAA's Coast Watch portal for availing SeaWiFS 8-day composite chlorophyll-a data. ROMS model-simulated data presented in this paper are archived at central data repository of www.incois.gov.in and are available for research purposes; please contact kunal.c@incois.gov.in. This is INCOIS, CMLRE, and NIO contribution nos. 326, 97, and 6285, respectively.

De Vos, A., Pattiaratchi, C., & Wijeratne, E. (2013). Surface circulation and upwelling patterns around Sri Lanka. *Biogeosci Discuss*, *10*, 14,953–14,998.

Fairall, C. W., Bradley, E. F., Godfrey, J. S., Wick, G. A., Edson, J. B., & Young, G. S. (1996). Cool-skin and warm-layer effects on sea surface temperature. *Journal of Geophysical Research*, *101*(C1), 1295–1308. https://doi.org/10.1029/95JC03190

Fairall, C. W., Bradley, E. F., Rogers, D. P., Edson, J. B., & Young, G. S. (1996). Bulk parameterization of air-sea fluxes for tropical ocean-global atmosphere coupled-ocean atmosphere response experiment. *Journal of Geophysical Research*, *101*(C2), 3747–3764. https://doi.org/10.1029/95JC03205

Fennel, K., Hu, J., Laurent, A., Marta-Almeida, M., & Hetland, R. (2013). Sensitivity of hypoxia predictions for the northern gulf of Mexico to sediment oxygen consumption and model nesting. *Journal of Geophysical Research: Oceans*, *118*, 990–1002. https://doi.org/10.2112/SI63-008.1

Fennel, K., Wilkin, J., Levin, J., Moisan, J., O'Reilly, J., & Haidvogel, D. (2006). Nitrogen cycling in the Middle Atlantic Bight: Results from a three-dimensional model and implications for the North Atlantic nitrogen budget. *Global Biogeochem Cycles*, *20*, GB3007. https://doi.org/10.1029/2005GB002456

Fennel, K., Wilkin, J., Previdi, M., & Najjar, R. (2008). Denitrification effects on air-sea CO_2 flux in the coastal ocean: Simulations for the northwest North Atlantic. *Geophysical Research Letters*, *35*, L24608. https://doi.org/10.1029/2008GL036147

Goyet, C., Millero, F., O'Sullivan, D., Eischeid, G., McCue, S., & Bellerby R. (1998). Temporal variations of pCO_2 in surface seawater of the Arabian Sea in 1995. *Deep Sea Research Part I: Oceanographic Research Papers*, *45*(4-5), 609–623.

Griffies, S. M., & Hallberg, R. W. (2000). Biharmonic friction with a Smagorinsky-like viscosity for use in large-scale eddy-permitting ocean models. *Monthly Weather Review*, *128*(8), 2935–2946.

Gupta, G. V. M., Sudheesh, V., Sudharma, K., Saravanane, N., Dhanya, V., Dhanya, K., et al. (2016). Evolution to decay of upwelling and associated biogeochemistry over the southeastern Arabian Sea shelf. *Journal of Geophysical Research: Biogeosciences*, *121*, 159–175. https://doi.org/10.1002/2015JG003163

Haidvogel, D. B., Arango, H., Budgell, W. P., Cornuelle, B. D., Curchitser, E., Di Lorenzo, E., et al. (2008). Ocean forecasting in terrain-following coordinates: Formulation and skill assessment of the Regional Ocean Modeling System. *Journal of Computational Physics*, *227*(7), 3595–3624.

Jyothibabu, R., Vinayachandran, P., Madhu, N., Robin, R., Karnan, C., Jagadeesan, L., & Anjusha, A. (2015). Phytoplankton size structure in the southern Bay of Bengal modified by the summer monsoon current and associated eddies: Implications on the vertical biogenic flux. *Journal of Marine Systems*, *143*, 98–119.

Koné, V., Aumont, O., Lévy, M., & Resplandy, L. (2009). Physical and biogeochemical controls of the phytoplankton seasonal cycle in the Indian ocean: A modeling study. *Indian Ocean Biogeochemical Processes and Ecological Variability*, *185*, 147–166.

Large, W. G., McWilliams, J. C., & Doney, S. C. (1994). Oceanic vertical mixing: A review and a model with a nonlocal boundary layer parameterization. *Reviews of Geophysics*, *32*(4), 363–403.

Lévy, M., Lengaigne, M., Bopp, L., Vincent, E. M., Madec, G., Éthé, C., et al. (2012). Contribution of tropical cyclones to the air-sea CO_2 flux: A global view. *Global Biogeochemical Cycles*, *26*, GB2001. https://doi.org/10.1029/2011GB004145

Lévy, M., Shankar, D., André, J.-M., Shenoi, S., Durand, F., & de Boyer Montégut, C. (2007). Basin-wide seasonal evolution of the Indian Ocean's phytoplankton blooms. *Journal of Geophysical Research*, *112*, C12014. https://doi.org/10.1029/2007JC004090

Liu, W. T., Katsaros, K. B., & Businger, J. A. (1979). Bulk parameterization of air-sea exchanges of heat and water vapor including the molecular constraints at the interface. *Journal of the Atmospheric Sciences*, *36*(9), 1722–1735. https://doi.org/10.1175/1520-0469(1979)036<1722:BPOASE>2.0.CO;2

Louanchi, F., Metzl, N., & Poisson, A. (1996). Modelling the monthly sea surface fCO_2 fields in the Indian ocean. *Marine Chemistry*, *55*(3-4), 265–279.

Madhupratap, M., Gauns, M., Ramaiah, N., Kumar, S. P., Muraleedharan, P., de Sousa, S., et al. (2003). Biogeochemistry of the Bay of Bengal: Physical, chemical and primary productivity characteristics of the central and western Bay of Bengal during summer monsoon 2001. *Deep Sea Research Part II: Topical Studies in Oceanography*, *50*(5), 881–896. https://doi.org/10.1016/S0967-0645(02)00611-2,bay of Bengal

Millero, F. J., Lee, K., & Roche, M. (1998). Distribution of alkalinity in the surface waters of the major oceans. *Marine Chemistry*, *60*(1-2), 111–130.

Prasanna Kumar, S., Muraleedharan, P., Prasad, T., Gauns, M., Ramaiah, N., De Souza, S., et al. (2002). Why is the Bay of Bengal less productive during summer monsoon compared to the Arabian Sea? *Geophysical Research Letters*, *29*(24), 2235. https://doi.org/10.1029/2002GL016013

Prasanna Kumar, S., Nuncio, M., Narvekar, J., Kumar, A., Sardesai, S., De Souza, S., et al. (2004). Are eddies nature's trigger to enhance biological productivity in the Bay of Bengal? *Geophysical Research Letters*, *31*, L07309. https://doi.org/10.1029/2003GL019274

Rajagopal, E. N., Iyengar, G. R., George, J. P., Gupta, M. D., Mohandas, S., Siddharth, R., et al. (2012). Implementation of unified model based analysis-forecast system at NCMRWF. *NMRF/TR/2/2012*, 1–45.

Ravichandran, M., Behringer, D., Sivareddy, S., Girishkumar, M., Chacko, N., & Harikumar, R. (2013). Evaluation of the Global Ocean Data Assimilation System at INCOIS: The tropical Indian Ocean. *Ocean Modelling*, *69*, 123–135.

Redfield, A. C., Ketchum, B. H., & Richards, F. A. (1963). The influence of organisms on the composition of sea-water. In M. N. Hill (Ed.), *The Sea* (Vol. 2). New York, NY: Wiley.

Sabu, P., Devi, C. A., Lathika, C., Sanjeevan, V., & Gupta, G. V. M. (2015). Characteristics of a cyclonic eddy and its influence on mesozooplankton community in the northern Bay of Bengal during early winter monsoon. *Environmental monitoring and assessment*, *187*(6), 1–19.

Sarma, V. V. S. S., Krishna, M., Paul, Y., & Murty, V. (2015). Observed changes in ocean acidity and carbon dioxide exchange in the coastal Bay of Bengal—A link to air pollution. *Tellus B*, *67*, 24638.

Sarma, V. V. S. S., Krishna, M., Rao, V., Viswanadham, R., Kumar, N., Kumari, T., et al. (2012). Sources and sinks of CO_2 in the west coast of Bay of Bengal. *Tellus B: Chemical and Physical Meteorology*, *64*(1), 10,961.

Sarma, V. V. S. S., Kumar, M. D., Gauns, M., & Madhupratap, M. (2000). Seasonal controls on surface pCO_2 in the central and eastern Arabian Sea. *Journal of Earth System Science*, *109*(4), 471–479.

Sarma, V. V. S. S., Lenton, A., Law, R., Metzl, N., Patra, P. K., Doney, S., et al. (2013). Sea-air CO2 fluxes in the Indian ocean between 1990 and 2009. *Biogeosciences*, *10*, 7035–7052.

Sarma, V. V. S. S., Rao, G., Viswanadham, R., Sherin, C., Salisbury, J., Omand, M. M., et al. (2016). Effects of freshwater stratification on nutrients, dissolved oxygen, and phytoplankton in the Bay of Bengal. *Oceanography*, *29*, 222–231. bay of Bengal.

Sharada, M., Swathi, P., Yajnik, K., & Devasena, C. K. (2008). Role of biology in the air-sea carbon flux in the Bay of Bengal and Arabian Sea. *Journal of Earth System Science*, *117*(4), 429–447.

Shulman, I., Kindle, J. C., DeRada, S., Anderson, S. C., & Pentam, B. (2003). Development of a hierarchy of nested models to study the California current system. In *Estuarine and Coastal Modeling* (pp. 16). California, USA: ASCE.

Takahashi, T., Sutherland, S. C., Wanninkhof, R., Sweeney, C., Feely, R. A., Chipman, D. W., et al. (2009). Climatological mean and decadal change in surface ocean pCO_2, and net sea–air CO_2 flux over the global oceans. *Deep Sea Research Part II: Topical Studies in Oceanography*, *56*(8-10), 554–577.

Takeshita, Y., Martz, T. R., Johnson, K. S., Plant, J. N., Gilbert, D., Riser, S. C., et al. (2013). A climatology-based quality control procedure for profiling float oxygen data. *Journal of Geophysical Research: Oceans*, *118*, 5640–5650. https://doi.org/10.1002/jgrc.20399

Udayshankar, S. (2015). Statistical process control (Spc) in a high volume machining center: Value of standard operating procedures (PhD thesis), Massachusetts Institute of Technology.

Valsala, V., & Maksyutov, S. (2013). Interannual variability of the air–sea CO_2 flux in the north Indian Ocean. *Ocean Dynamics*, *63*(2-3), 165–178.

Vidya, P., & Kumar, S. P. (2013). Role of mesoscale eddies on the variability of biogenic flux in the northern and central Bay of Bengal. *Journal of Geophysical Research: Oceans*, *118*, 5760–5771. https://doi.org/10.1002/jgrc.20423

Vinayachandran, P., Chauhan, P., Mohan, M., & Nayak, S. (2004). Biological response of the sea around Sri Lanka to summer monsoon. *Geophysical Research Letters*, *31*, L01302. https://doi.org/10.1029/2003GL018533

Vos, A. d., Pattiaratchi, C., & Wijeratne, E. (2014). Surface circulation and upwelling patterns around Sri Lanka. *Biogeosciences*, *11*(20), 5909–5930.

Zeebe, R., & Wolf-Gladrow, D. (2001). *CO_2 in seawater: Equilibrium, Kinetics, Isotopes, Elsevier Oceanogr. Ser.* (Vol. 65). Amsterdam: Elsevier.